



# Design and characterization of multi-stable mechanical metastructures with level and tilted stable configurations



Yong Zhang\*, Qi Wang, Marcel Tichem, Fred van Keulen

Department of Precision and Microsystems Engineering, Delft University of Technology, Mekelweg 2, 2628 CD, Delft, The Netherlands

## ARTICLE INFO

### Article history:

Received 15 July 2019

Received in revised form 18 October 2019

Accepted 18 October 2019

Available online 24 October 2019

### Keywords:

Metastructure

Multi-stability

Level stable configuration

Tilted stable configuration

Snap-through transition

## ABSTRACT

Multi-stable structures are able to achieve significant geometric change and retain specific deformed configurations after the loads have been removed. This reconfiguration property enables, for example, to design metamaterials with tunable features. In this work, a type of multi-stable metastructures exhibiting both level and tilted stable configurations is proposed based on 2D and 3D arrangements of bi-stable elements. The resulting level and tilted configurations are enabled by the rotational compliance, bi-stability and spatial arrangement of unit cells. The bi-stability of the unit cells and multi-stability of the metastructures are demonstrated and characterized by experiments and finite element analysis. Results show that transitions between level stable configurations are symmetric in terms of load-deflection response while switching to the tilted stable configurations leads to asymmetric mechanical responses. The tilted stable configurations are less stable than the level configurations. Moreover, we demonstrate that the level and tilted stable configurations of the metastructure depend on the parallel and serial arrangement of the unit cells.

© 2019 The Author(s). Published by Elsevier Ltd. This is an open access article under the CC BY license (<http://creativecommons.org/licenses/by/4.0/>).

## 1. Introduction

Mechanical metamaterials are rationally designed structured materials whose macroscopic properties are mainly determined by their structures rather than composition [1,2]. This allows to realize unusual and novel properties for metamaterials. For example, mechanism-based auxetic metamaterials have been designed to obtain deployable structures [3,4]. Phononic metamaterials have been developed to control and prohibit elastic waves in specific frequency ranges [5–7]. Other unconventional properties include ultra-lightweight but high stiffness [8], negative compressibility transitions [9] and high energy absorption [10].

In order to tune the properties of metamaterials after fabrication, metamaterials composed of multi-stable metastructures have been proposed and actively explored in recent years [11]. Multi-stable structures have multiple stable morphologies and are able to achieve significant geometrical changes by switching between different stable configurations. More importantly, these stable configurations do not require external loads to be maintained. The multi-stability has mainly been utilized in design of shape-changing structures and energy absorbers with tunable stiffness [12–15].

Many studies have demonstrated the design of multi-stable metastructures based on bi-stable elements exhibiting snap-

through behavior. These designed structures are normally referred to as snap-through induced multi-stable structures (SIMS) [16–19]. Within the elastic regime, snap-through is a type of instability that causes a structure to jump from one stable configuration to the other when external loads beyond critical values are applied [20]. Thus, two stable configurations can be accommodated [21,22]. The principle of snap-through based bi-stability can be applied to design smart metastructures over a wide range of length scales [11]. By combining bi-stable elements, multi-stability can be realized for metastructures [23–29]. For instance, Restrepo et al. [24] developed metastructures consisting of an array of bi-stable camber beams which can absorb energy under cyclic loading. Shan et al. [25] proposed a multi-stable structure using inclined straight beams for trapping elastic energy. Santer et al. [30] presented a multi-stable mechanism to morph surfaces. Since all the unit cells within the SIMS are identical, the deformation sequence is unpredictable when the structure is uniformly loaded. Che et al. [26] introduced geometry and material variations to acquire programmable behavior. Moreover, this snap-through behavior can also be triggered under tensile loading besides compressive loads [31].

Most studies on multi-stable metastructures are limited to translational state changes and only level stable configurations are explored due to the constraint of unit cells' rotational compliance. In this work, we demonstrate a new type of three-dimensional (3D) multi-stable metastructure allowing for both level and tilted stable configurations. 3D bi-stable unit cells with

\* Corresponding author.

E-mail address: [Y.Zhang-15@tudelft.nl](mailto:Y.Zhang-15@tudelft.nl) (Y. Zhang).

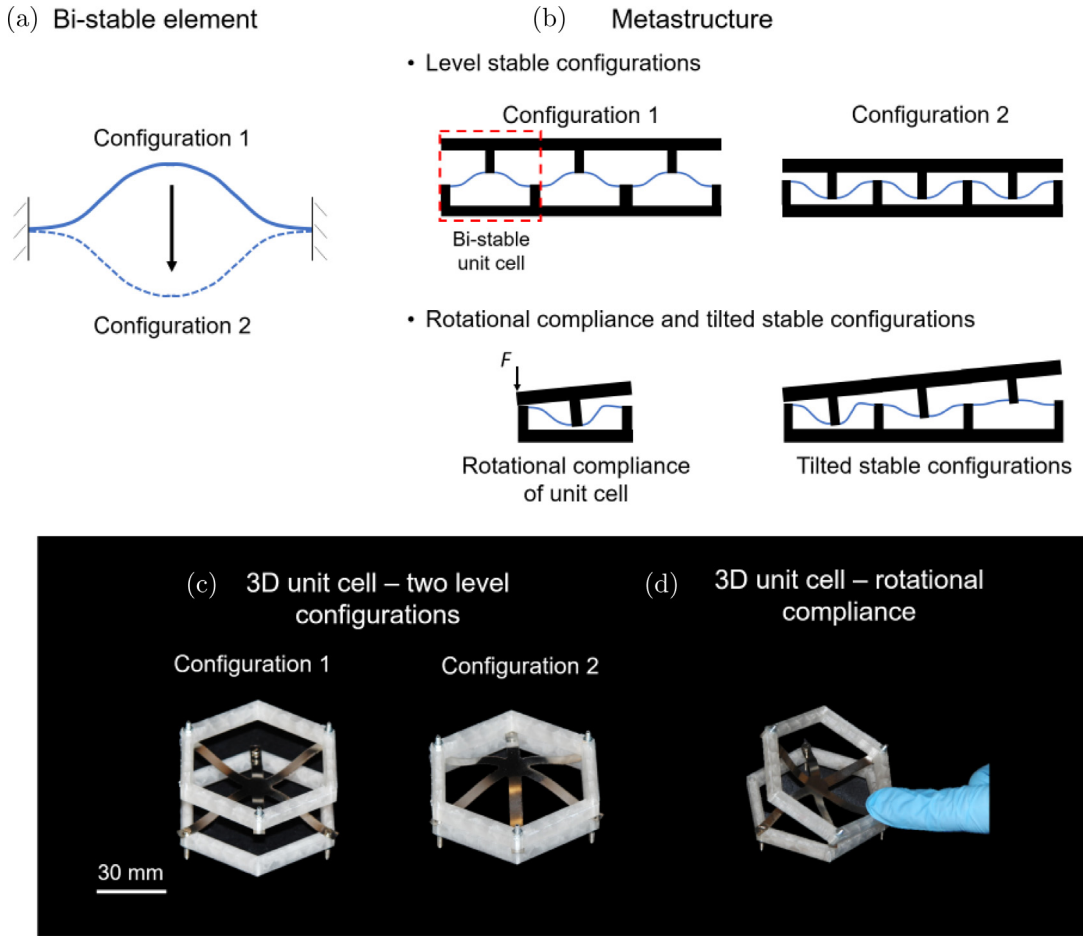


**Fig. 1.** Design of 3D bi-stable unit cells. (a) A schematic of bi-stable behavior. (b) Schematics of a multi-stable metastructure exhibiting level stable configurations and rotational compliance. (c) The proposed 3D bi-stable unit cell with two level stable configurations. (d) Rotational compliance of the unit cell.

snap-through behavior and rotational compliance are designed first. By a specific assembly of a number of unit cells, the resulting multi-stable metastructure is able to exhibit both translational and rotational macroscopic degrees of freedom (DOFs). That is, the resulting structures possess multiple equilibrium states, including level and tilted stable configurations. These additional tilted stable configurations offer more design freedom for motion-related applications. Moreover, various tilted stable configurations can be obtained by combining the unit cells in different arrangements, which makes it possible to control the multi-stable property of metamaterials.

This paper is organized as follows. Section 2 describes the geometry of the proposed unit cells and resulting multi-stable metastructures. The main features of the unit cells are highlighted and the associated level and tilted stable configurations are demonstrated. Section 3 describes experimental and numerical methods adopted in this work. The snap-through behavior of the proposed unit cells and the multi-stable metastructures are characterized in Section 4. In Section 5, the influence of unit cell arrangements on the resulting multi-stable behavior is studied. Conclusions are presented in Section 6.

## 2. Structure design

In this study, we are targeting multi-stable metastructures, where bi-stable elements are used as basic unit cells. As shown in Fig. 1(a), a single bi-stable element allows for translational motion by switching among two stable configurations. The 1D arrangement of these elements forms a metastructure with two

level stable configurations (LSCs), as illustrated in Fig. 1(b). The corresponding metastructure may exhibit a relatively large stroke via transition between LSCs. If, in addition, the bi-stable unit cell provides rotational compliance, then it may be possible for the metastructure to exhibit additional tilted stable configurations (TSCs) next to the intrinsic LSCs (see Fig. 1(b)).

For a design of 3D bi-stable units, the rotational compliance and bi-stable behavior are needed as well. Accordingly, a 3D unit cell with these two properties was proposed and studied, as depicted in Fig. 1(c). Specifically, a leaf spring with six strips (six-strip structure) was prestressed into a 3D curved shape by using two smaller frames. When this unit cell (Configuration 1) is mechanically deformed, the curved six-strip structure reconfigures into the other level stable configuration (Configuration 2), which results in a translation motion, see Fig. 1(c). Meanwhile, the rotational compliance ensures that the unit cell can achieve angular deformation, as shown in Fig. 1(d).

After combining the proposed unit cells into a metastructure, it can be observed in Fig. 2(a) that four stable configurations can be achieved for a metastructure composed of two unit cells: level (Configuration 1 and 4) and tilted stable configurations (Configuration 2 and 3). When unloaded, the metastructure can maintain its deformed shape in either level or tilted state. Different stable configurations can be realized by applying different loading conditions. For example, when the demonstrated metastructure is loaded in a LSC symmetrically, it responds with a translational transition to switch between two LSCs (Configuration 1 or 4). However, when an asymmetric load is applied, it transforms to a tilted stable configuration (Configuration 2 or 3).

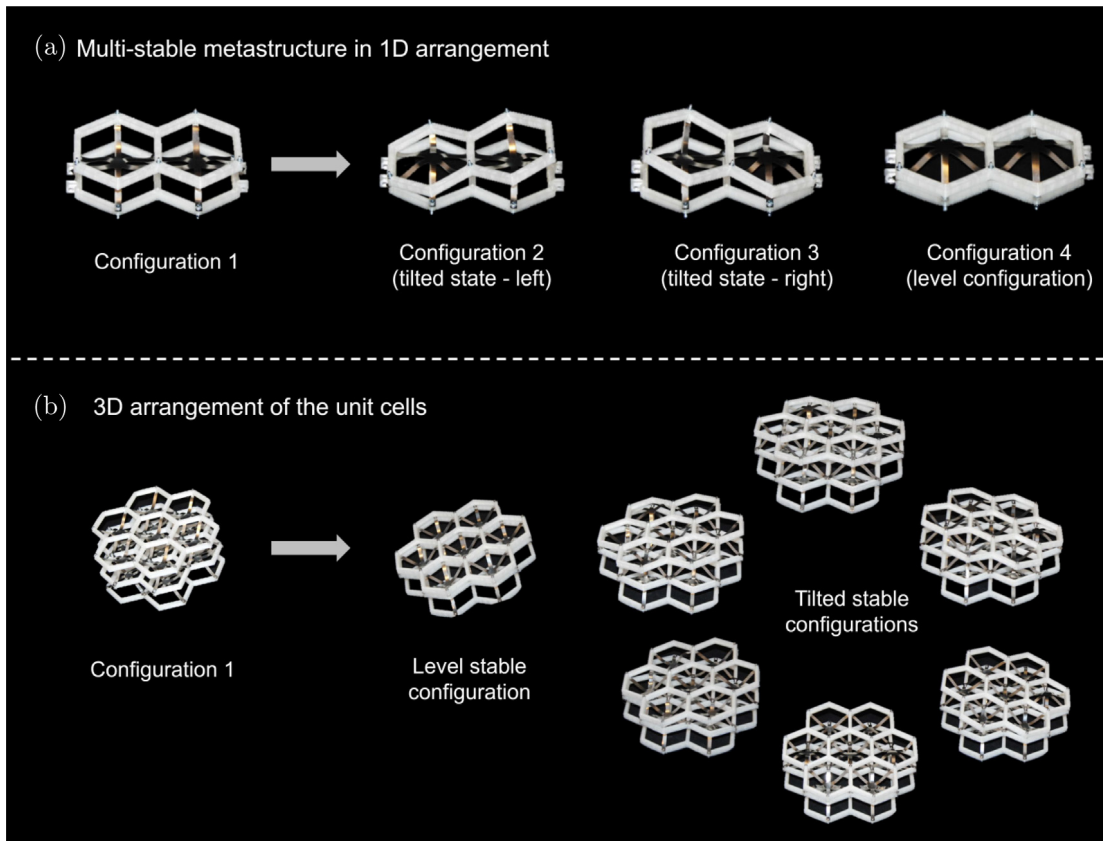


**Fig. 2.** The proposed metastructures showing both level and tilted stable configurations. (a) A multi-stable metastructure consisting of two cells is obtained by 1D arrangement. Four stable states are found including LSCs and TSCs. (b) A 3D arrangement of unit cells resulting in multiple TSCs and LSCs.

Based on the proposed unit cells, it is possible to obtain different arrangements by repeating the unit cells. By a 3D arrangement of the unit cells, the resulting metastructure may have multiple TSCs along different directions. As an example, each layer of the arranged metastructure shown in Fig. 2(b) is able to exhibit six TSCs with different tilting orientations and two LSCs along the vertical direction (see the Supplementary video). It should be noted that which particular level and tilted stable configurations can be realized depend on: (i) the nonlinear properties of the unit cells, in particular their bi-stable behavior and rotational compliance; (ii) the spatial arrangement of the unit cells. In order to identify the influence of arrangement on multi-stability, the mechanical responses of metastructures with different arrangements are experimentally determined, as discussed in Section 5.

### 3. Methods

#### 3.1. Fabrication

Samples were manufactured following the procedure as illustrated in Fig. 3(a)–(d). The bi-stable unit cell is composed of three components, namely two frames and the six-strip structure. The flat six-strip structures were fabricated by laser-cutting 0.1 mm thick spring steel sheets (Alloy 1.4310, Jeveka, The Netherlands). The frames were printed from polylactic acid (PLA) using a fused deposition modeling printer (Prusa i3 MK2) and have been considered rigid in the numerical simulations. By connecting the frames with smaller in-plane dimensions, the six-strip structure was buckled into a curved configuration and the unit cell was assembled using screws as fasteners. The metastructures were obtained by connecting unit cells in different directions.

**Table 1**  
Geometric parameters of bi-stable unit cells.

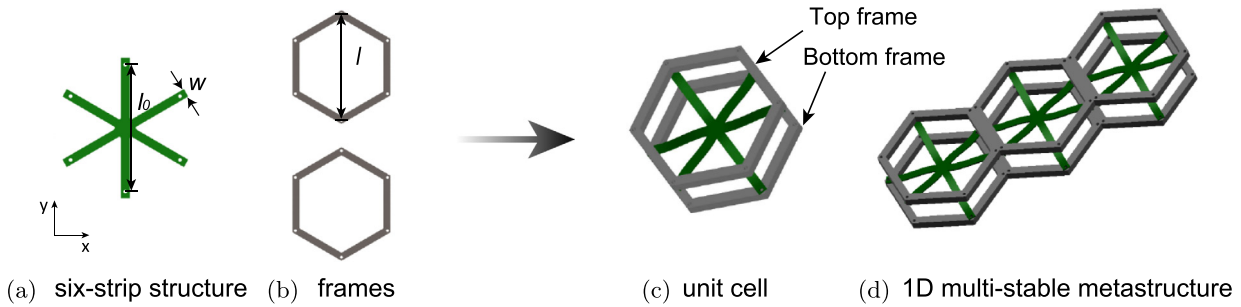
Parameters	w	l <sub>0</sub>	l	t <sub>e</sub>	t <sub>f</sub>
Values (mm)	5	73	69	0.1	6

Fig. 3(d) illustrates an example of a 1D combination of unit cells for a multi-stable metastructure. Table 1 lists the geometric parameters of samples in this study.

#### 3.2. Experiments and simulations

To characterize the snap-through transitions, we investigated the mechanical behavior of structures using a uniaxial testing machine (ZwickRoell Z005, Germany). Uniaxial compression and tensile tests were conducted on fabricated samples to capture their snap-through transitions. Connectors were printed and used to transfer loading forces during loading tests. Quasi-static conditions were applied using a displacement control at a loading rate of 10 mm min<sup>-1</sup>. During the mechanical deformation of the structures, we quantified the snap-through transitions as force-deflection curves. All the tests and measurements shown in this paper were repeated three times for each sample. For each design, three samples were fabricated and tested to get mean values.

Nonlinear finite element analysis (FEA) was performed using ABAQUS to investigate in detail the local deformation of the designed structures. Because the strips experience only small deformations, a linear elastic constitutive model was used in the FEA. Four-node shell elements with reduced integration (S4R) were employed for the thin six-strip structure with Young's modulus  $E = 180$  GPa and Poisson's ratio  $\nu = 0.29$ , consistent with the material we used in experiments. Frames were meshed



**Fig. 3.** Schematics for fabrication of the presented unit cells and metastructures. (a) The flat six-strip element with an out-of-plane thickness  $t_e$  and its in-plane geometric parameters. (b) 3D printed frames with an out-of-plane thickness  $t_f$  and in-plane dimensions. (c) Assemble the bi-stable unit cell by connecting the six-strip structure to the two frames. (d) An assembly of the unit cells to obtain a multi-stable metastructure.

using eight-node linear brick, reduced integration solid elements (C3D8R). A relatively high Young's modulus was assigned to the frames to mimic their rigidity. Pre-stresses were introduced to the metastructure by thermal loads. Specifically, thermal expansion coefficients were assigned to the top and bottom frames. By applying a controlled temperature drop, the frames shrank and resulted in the desired initial configuration of the modeled metastructures. The detailed modeling procedure we followed can be found in the supplementary data.

#### 4. Mechanical properties of transitions into LSCs and TSCs

In this section, the mechanical properties of the designed unit cell as well as the associated metastructures are presented. The bi-stability of the unit cells and multi-stability of the metastructures are quantified, respectively. The results of experimental characterization will be given and discussed along with the numerical analysis.

##### 4.1. Bi-stability of the unit cell

To measure the responses of the presented unit cell under uniaxial loads, we firstly compressed the unit cell to Configuration 2 (denoted as loading) and then pulled it back to Configuration 1 (denoted as unloading), as depicted in Fig. 4(a)–(b). Main mechanical characteristics can be observed in Fig. 4(b): (i) The bi-stable deformation behavior is evident from the force–deflection curve. In the initial phase, the force gradually increases along with the axial displacement until the maximum critical compression force ( $F_{max}$ ) is reached, as plotted in Fig. 4(b). A further deformation triggers elastic instability (i.e. snapping), where the structure shows negative stiffness. During the snapping phase, the force initially reduces to zero, and then becomes negative (tension). When contact between top and bottom frames occurs at a certain displacement (represented as the vertical dashed line in Fig. 4(b)), the negative force is balanced by the contact force, leading to the Configuration 2. (ii) Symmetric behavior is observed, meaning that  $F_{max}$  is almost equal to that of the maximum tensile force (referred to  $F_{min}$  in Fig. 4(b)). This is due to the fact that the pre-stress is introduced to the flat six-strip structure. Similar behavior is also observed in other pre-stressed bi-stable designs in literature [32,33]. (iii) The reverse unloading process (black curve) follows nearly the same path as the loading (red curve), which demonstrates that the hysteresis is negligible for these structures.

In comparing numerical and experimental results, good agreement is observed before the contact occurs, as seen in Fig. 4(b). Since the frames are considered rigid, only the six-strip structure of the unit cell is modeled in FEA. It can be seen in Fig. 4(b) that the simulation reproduces the snapping response in experiments before the contact. The mismatch at the contact phase can be

explained by the fact that the contact is not considered in simulations and thus, the six-strip structure is deformed further into the symmetric Configuration 2. In addition, the symmetric transition behavior is also demonstrated by the stress distributions in Fig. 4(c) and (d), where the two stable configurations correspond to the same level of strain energy.

##### 4.2. Multi-stability of the metastructure

The metastructures allowing for level and tilted configurations were characterized with representative samples which are 1D combination of two unit cells, as shown in Fig. 5(a). The loading response between LSCs is displayed in Fig. 5(b). It can be expected that compared to the snap-through of one unit cell, the critical force of this metastructure doubles while the maximal displacement remains unchanged. The characteristics of snapping transition are similar to the expected results, where the average  $F_{max}$  is around 2.8 N. In addition, integrating the force–deflection curve over the region of positive force and negative force (denoted as  $E_{in}$  and  $E_{out}$  in Fig. 5(b)), we find that  $E_{in}$  is almost equal to  $E_{out}$  as a result of the symmetric transition.

The transition to TSCs was realized by applying loads on one side of the top frame. The metastructure snaps from the initial to tilted configurations, as displayed in Fig. 6(a)–(b). Similarly, after the process of snapping and contact, the metastructure stabilizes at the TSC without external loads. This snapping behavior differs from the snapping behavior of the level configuration in two aspects: (i) The critical compression force  $F_{max}$  (1 N in Fig. 6(b)) is smaller than that of LSCs (2.8 N in Fig. 5(b)). Therefore, less force/energy is required for the metastructure to switch into TSCs while the transition to LSCs requires larger actuation force. (ii) The snapping response shown in Fig. 6(b) is not symmetric because curves in compression (positive) and tension (negative) loading are obviously different. The critical tension force  $F_{min}$  ( $-0.5$  N) is lower as compared to  $F_{max}$  (1 N), indicating that the TSCs are less stable than the corresponding LSCs. This can also be explained from an energy perspective. It can be observed that  $E_{out}$  in Fig. 6(b) is much smaller than  $E_{in}$ , implying that energy is trapped within the deformed stable TSCs. Therefore, when snapping to TSCs, the strips locally reconfigure to a higher energy, yet stable deformed state.

The corresponding numerical result agrees well with the experimental measurement, as plotted in Fig. 6(b). The stress evolution in Fig. 6(c)–(e) shows that the first cell experiences relatively larger deformation than the second cell. In particular, the three top strips (1,3,5) in the first cell snap into the other configuration during the initial loading stage. When this metastructure reaches the state as illustrated in Fig. 6(e), the Strip 3 already snapped to the other side. However, the Strip 1 and 5 have not been snapping fully. High stresses can be found in Strip 1 and 5, as shown in Fig. 6(e). The overall equilibrium of the tilted stable state can be

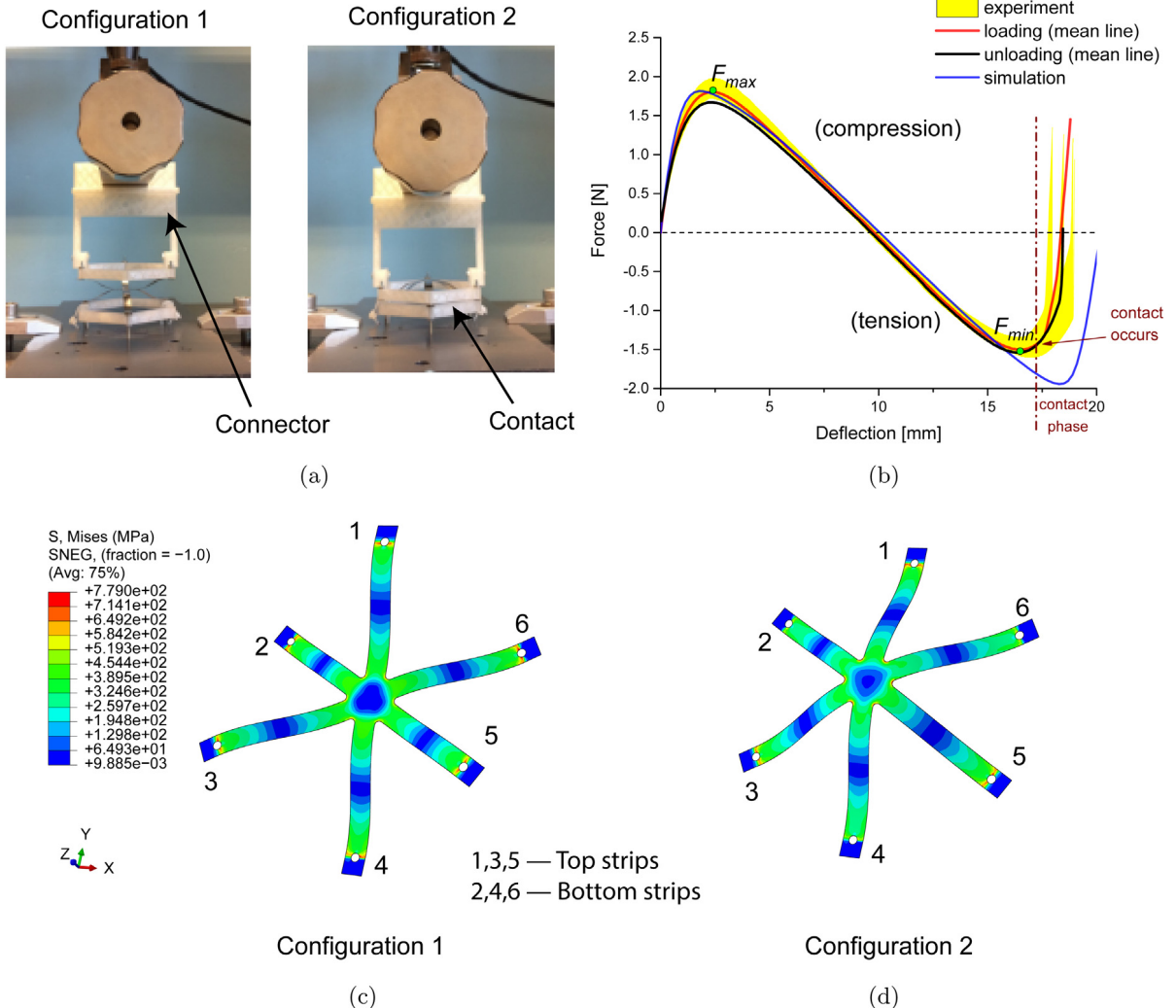


**Fig. 4.** Snap-through behavior of the bi-stable unit cell. (a) The two stable configurations in experimental measurements. (b) Force-deflection curves for snap-through transitions between Configuration 1 and 2. The red and black curves represent the mean values of multiple experimental tests (yellow area) for loading and unloading, respectively. The dashed vertical line (contact) represents the situation that during loading, the top frame is in contact with the bottom frame. Blue curve denotes the snapping response obtained from FEA. (c)–(d) Contour plots for von Mises stress of the unit cell at Configuration 1 and 2, respectively. (For interpretation of the references to color in this figure legend, the reader is referred to the web version of this article.)

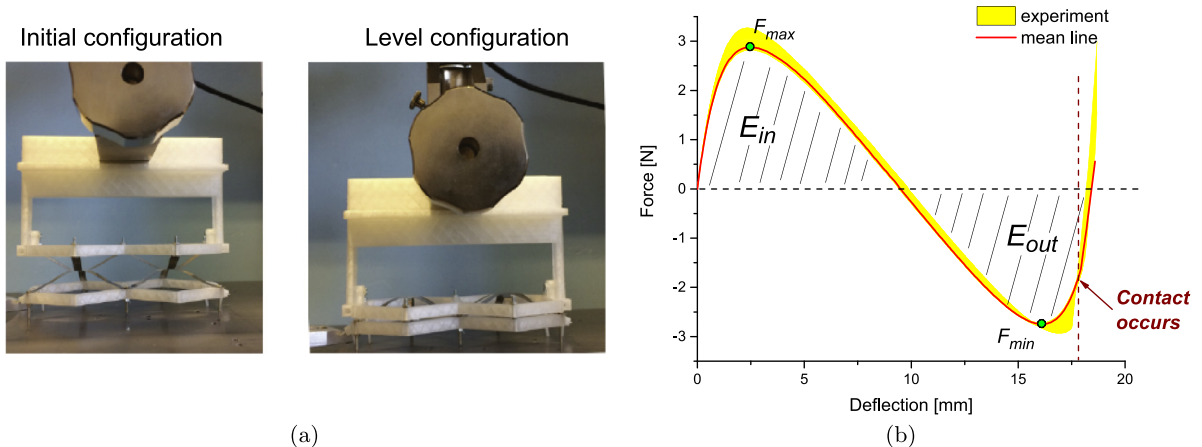


**Fig. 5.** Characterization of snapping transitions from the initial configuration to the other level stable configuration for a metastructure composed of two bi-stable elements. (a) Two LSCs: initial and deformed level configurations. (b) Force-deflection curves corresponding to the snapping from the initial to level configuration. Red curve shows the mean values of multiple measurements.

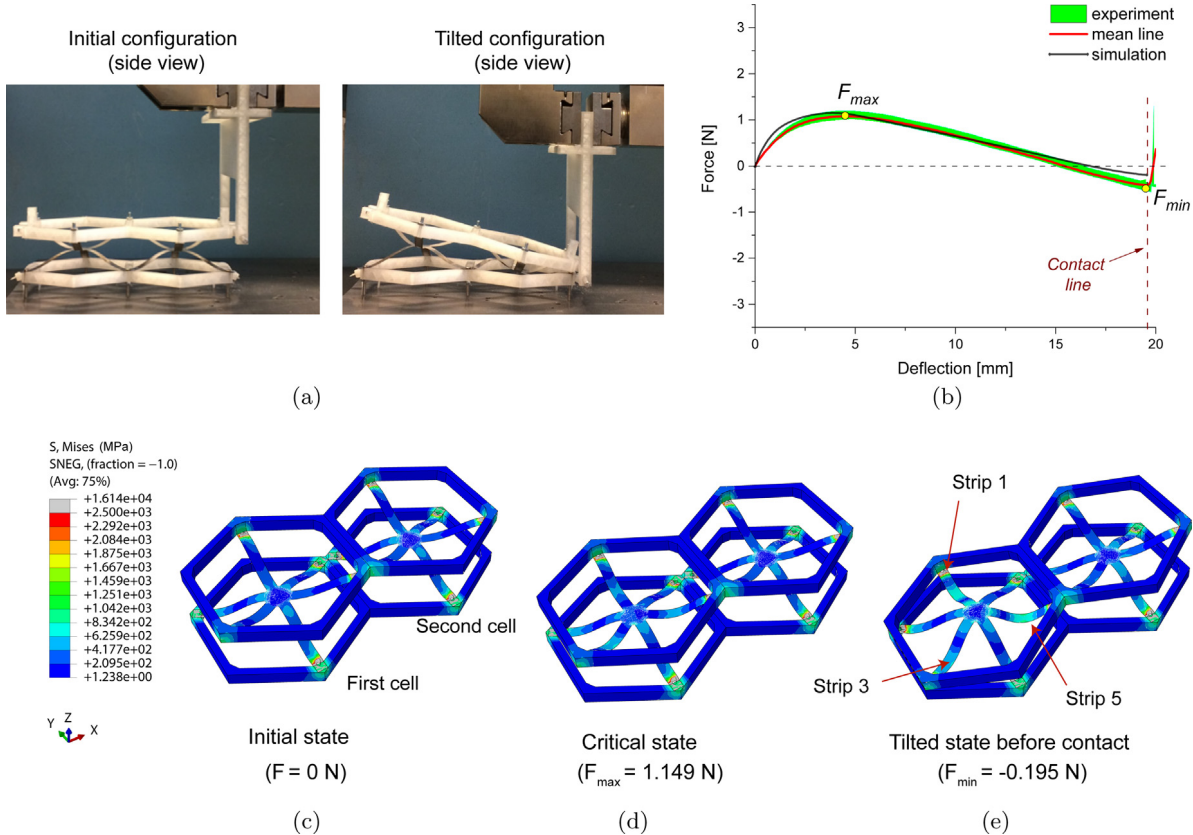


**Fig. 6.** The tilting transitions of metastructures by experimental and numerical characterizations. (a) The initial configuration and the deformed tilted configuration. (b) Force–deflection diagrams for transitions from the initial to tilted configuration. Red line displays mean values of experimental results (green area); numerical result is plotted as black line. (c)–(e): FEA of snapping transitions: (c) represents the initial configuration of this metastructure. Then, the structure is loaded on the left side and (d) depicts the critical state where the maximum compression force  $F_{max}$  is reached. The stress distribution of the tilted state before the contact is shown in (e). (For interpretation of the references to color in this figure legend, the reader is referred to the web version of this article.)

interpreted as a combination of three force components: upward contact force from the bottom frame; downward pushing force applied by the first cell and upward pulling force generated in the second cell. A simplified analytical model for capturing the tilting transitions can be further developed based on the force equilibrium in future.

## 5. Metastructures with different arrangements

Here, two main arrangements of combining bi-stable mechanisms are studied and demonstrated: parallel in either one or two directions (1D and 2D), and serial arrangements. The serial arrangement represents the case of stacking bi-stable unit cells on top of each other, where the load is equally resisted by all unit cells but with different deformations for each. A parallel arrangement helps synthesizing new multi-stable characteristics from existing bi-stable units and it can be realized by in-plane patterning of the unit cells. Since the LSCs will be similar to the behavior discussed in previous section thus, from here on the main focus will be on the TSCs.

### 5.1. Parallel arrangement: 1D

Metastructures with unit cells arranged in 1D are depicted in Fig. 7(a). Fig. 7(b) depicts multiple force–deflection responses for switching from the initial configuration to different TSCs shown in Fig. 7(a). It is first found that these metastructures are able to exhibit TSCs, which is also demonstrated by experimental results shown in Fig. 7(b). Fig. 7(c) presents the critical compression forces  $F_{max}$  and the resulting tilt angle  $\theta$  (see Fig. 7(a)) at TSCs

as a function of cell numbers. Non-proportional relations are reported as a result of the nonlinear behavior of the unit cells. With increasing the number of cells, the critical compression force increases while the tilt angle decreases.

### 5.2. Parallel arrangement: 2D

The smallest 2D arrangement is composed of three unit cells, as seen in Fig. 8(a). Besides the stable initial and level configurations, multiple TSCs (i.e. tilting behavior along different directions) are realized for the metastructure. Furthermore, it is noted that the tilting axes depend on the in-plane symmetry of structure. As this structure has three axes of symmetry as shown in Fig. 8(a), we separate the TSCs into two categories: two-point tilting (Configuration 4,6,8) where there are two contact points at the TSCs and one-point tilting (Configuration 3,5,7) in which only one contact point is observed.

The characterization of snapping into LSCs and TSCs is displayed in Fig. 8(b) and (c), respectively. The snapping transition between LSCs shows a similar characteristic as the snap-through behavior of the unit cell. For the two-point tilting, the critical compression force is approximately two times larger than that of one-point tilting, as shown in Fig. 8(c). This can be explained by the fact that in case of two-point tilting two cells show snapping deflections whereas for one-point tilting, only the cell close to the loading point switches into the other stable configuration. The non-buckled unit cells mainly act as rotation points. The buckled unit cells essentially determine the snapping force of transitions. Moreover, the TSCs corresponding to the two-point tilting exhibit larger negative critical force ( $F_{min}$ ) as compared to the one-point

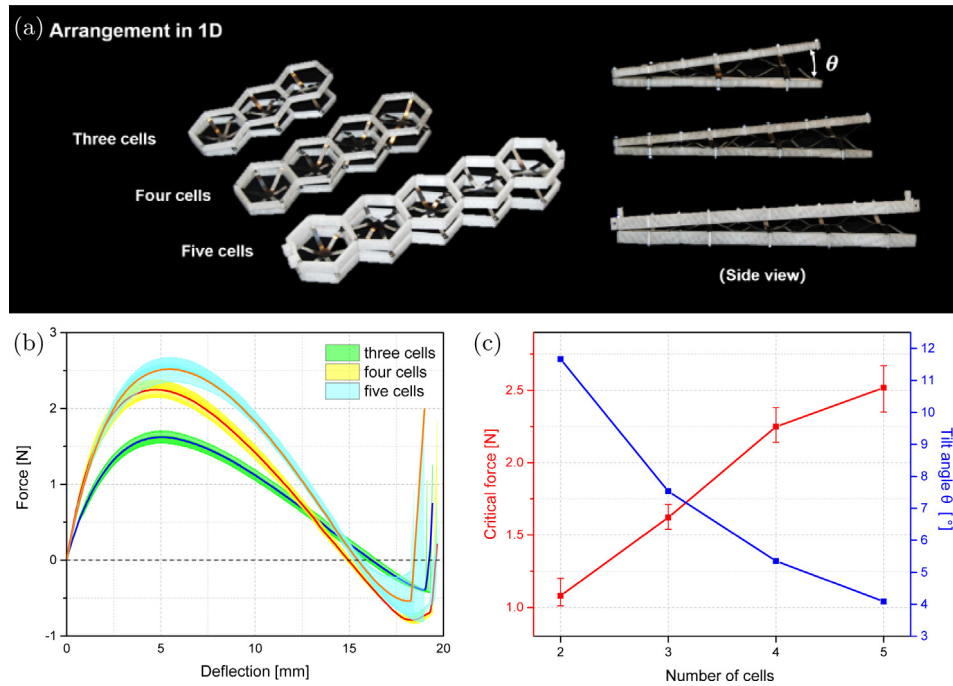


**Fig. 7.** The 1D parallel arrangement of the unit cells. (a) Metastructures consisting of three, four and five unit cells. (b) The tilting response of these 1D metastructures: loading from the initial configuration into TSCs experimentally. The solid curves represent the mean values. (c) The maximal critical compression forces ( $F_{\max}$ ) and tilt angles ( $\theta$ ) as a function of the number of unit cells.

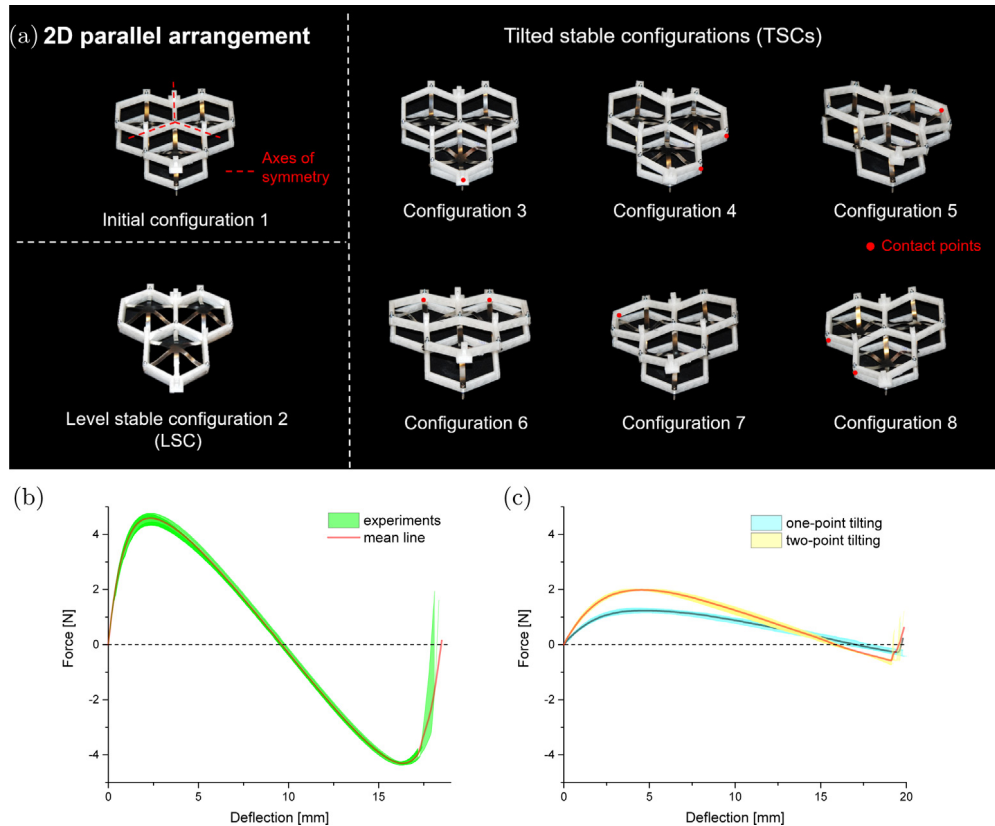


**Fig. 8.** A 2D parallel arrangement of metastructure and its stable configurations. (a) The stable configurations include six TSCs and two LSCs. Two types of TSCs are found for the metastructure: two-point and one-point tilting. (b) The experimental force–deflection response of snapping between LSCs (from Configuration 1 to 2). (c) The force–deflection diagrams for two types of snapping transitions in experiments: one-point tilting (from Configuration 1 to 3, 5 or 7) and two-point tilting (from Configuration 1 to 4, 6 or 8).

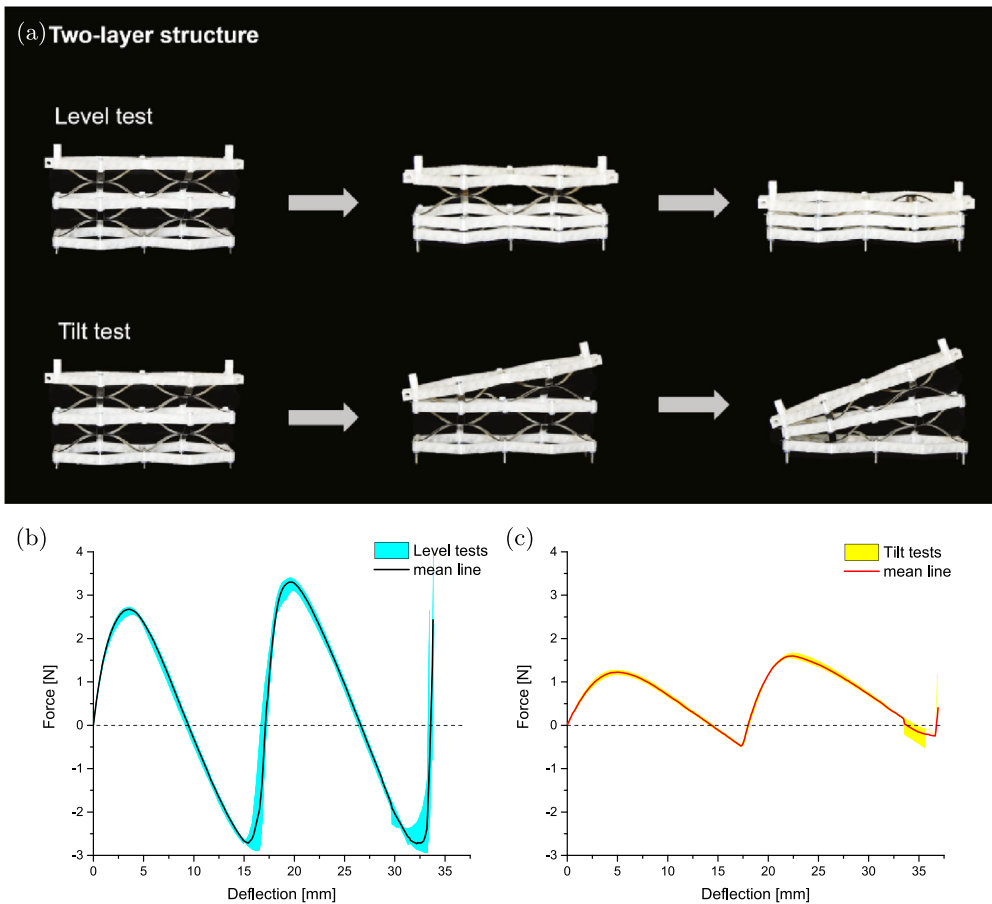


**Fig. 9.** A two-layer metastructure obtained by serial arrangements of the unit cells. (a) Five out of sixteen stable configurations for the two-layer metastructure. Experimental tests were conducted via uniform loading (level tests) and loading on the left side (tilt tests). (b) The mechanical response of level tests, namely the snapping transitions to LSCs. (c) The mechanical response of tilting tests, namely the snapping transitions to TSCs.

tilting, which implies that two-point TSCs are more stable than the one-point TSCs.

### 5.3. Serial arrangement

As discussed, the in-plane parallel arrangements mainly affect the tilting behavior and resulting stable configurations. The influence of assembling unit cells in series is studied through a metastructure with two layers, as displayed in Fig. 9(a). Specifically, each layer exhibits four stable configurations and the demonstrated two-layer structure can realize sixteen stable configurations in total. In general, by stacking elements with  $x$  stable configurations, the resulting  $n$  layers metastructure can possess  $x^n$  stable configurations. Here, we choose four typical stable configurations realized by applying different loading conditions, as shown in Fig. 9(a): level and tilt tests. These two tests denote the snap-through transitions to the LSCs and TSCs, respectively. The results of tests are plotted in Fig. 9(b)–(c). Two sequential snap-through responses are captured in both tests. The amplitude of the second peak force is slightly larger than the first one, although they are designed to be the same. Discrepancies arise from manufacturing imperfections and assembling tolerances. The fluctuation of force-deflection curves in a particular region may be caused by the loading or structural imperfections.

For the proposed bi-stable unit cells, the basic behavior of arrangements can be summarized as follows: (i) The 1D parallel arrangement results in two LSCs and TSCs with different tilting angles. (ii) For 2D in-plane symmetric patterning of the unit cells, the possible TSCs can be found based on the structural symmetry axes. (iii) By serial arrangements, more LSCs and TSCs can

be realized for the metastructure while each layer still exhibits multi-stable behavior independently. The presented multi-stable metastructures with various LSCs and TSCs can be further used as building blocks to construct multi-stable metamaterials. For instance, a multi-layer metamaterial can be formed as an assembly with both parallel and serial arrangements of the unit cell, as displayed in Fig. 2(b). Through controlling the layout of unit cells and the number of serial layers, the spatial positions and tilting angles of stable configurations can be tuned.

## 6. Conclusion

In this work, we have proposed a new type of 3D bi-stable unit cell which allows the corresponding metastructures to exhibit both level and tilted stable configurations (LSCs and TSCs respectively). The pre-stress gives rise to the LSCs and the rotational compliance of the unit cell paves the way for the TSCs. The snapping responses of the unit cells and metastructures were studied both experimentally and numerically. Results show that the transition to LSCs exhibits symmetric behavior in terms of maximal critical compression and tension force. Therefore, no energy is stored in the deformed configuration. For transitions to the TSCs, the load-deflection responses are asymmetric in such a way that the critical tension force is smaller than the maximal compression force, resulting in a deformed tilted stable state with higher strain energy. This indicates that TSCs are less stable when exposed to an external stimulus. Moreover, the metastructures are capable of exhibiting TSCs in multiple directions. Two main arrangements with different metastructures have been

demonstrated and studied. It has been shown that the tilting directions of in-plane symmetric patterning are determined by the symmetry axes of the metastructures while a number of LSCs can be accomplished by serial arrangements. Based on these arrangements, metastructures with multiple LSCs and TSCs can be designed and used to build reconfigurable metamaterials.

### Declaration of competing interest

The authors declare that they have no known competing financial interests or personal relationships that could have appeared to influence the work reported in this paper.

### Acknowledgments

Y. Zhang would like to thank China Scholarship Council (CSC NO. 201606120015) for the financial support.

### Appendix A. Supplementary data

Supplementary material related to this article can be found online at <https://doi.org/10.1016/j.eml.2019.100593>.

### References

- [1] T.A. Schaedler, W.B. Carter, Architected cellular materials, *Annu. Rev. Mater. Res.* 46 (2016) 187–210.
- [2] K. Bertoldi, V. Vitelli, J. Christensen, M. van Hecke, Flexible mechanical metamaterials, *Nature Rev. Mater.* 2 (11) (2017) 17066.
- [3] X. Ren, R. Das, P. Tran, T.D. Ngo, Y.M. Xie, Auxetic metamaterials and structures: a review, *Smart Mater. Struct.* 27 (2) (2018) 023001.
- [4] K. Bertoldi, P.M. Reis, S. Willshaw, T. Mullin, Negative poisson's ratio behavior induced by an elastic instability, *Adv. Mater.* 22 (3) (2010) 361–366.
- [5] M.I. Hussein, M.J. Leamy, M. Ruzzene, Dynamics of phononic materials and structures: historical origins, recent progress, and future outlook, *Appl. Mech. Rev.* 66 (4) (2014) 040802.
- [6] S. Babaei, N. Viard, P. Wang, N.X. Fang, K. Bertoldi, Harnessing deformation to switch on and off the propagation of sound, *Adv. Mater.* 28 (8) (2016) 1631–1635.
- [7] J. Meaud, K. Che, Tuning elastic wave propagation in multistable architected materials, *Int. J. Solids Struct.* 122 (2017) 69–80.
- [8] X. Zheng, H. Lee, T.H. Weisgraber, M. Shusteff, J. DeOtte, E.B. Duoss, J.D. Kuntz, M.M. Biener, Q. Ge, J.A. Jackson, et al., Ultralight, ultrastiff mechanical metamaterials, *Science* 344 (6190) (2014) 1373–1377.
- [9] Z.G. Nicolaou, A.E. Motter, Mechanical metamaterials with negative compressibility transitions, *Nature Mater.* 11 (7) (2012) 608.
- [10] J.-H. Lee, L. Wang, S. Kooi, M.C. Boyce, E.L. Thomas, Enhanced energy dissipation in periodic epoxy nanoframes, *Nano Lett.* 10 (7) (2010) 2592–2597.
- [11] K. Bertoldi, Harnessing instabilities to design tunable architected cellular materials, *Annu. Rev. Mater. Res.* 47 (2017) 51–61.
- [12] M.E. Pontecorvo, S. Barbarino, G.J. Murray, F.S. Gandhi, Bistable arches for morphing applications, *J. Intell. Mater. Syst. Struct.* 24 (3) (2013) 274–286.
- [13] D.M. Correa, C.C. Seepersad, M.R. Haberman, Mechanical design of negative stiffness honeycomb materials, *Integr. Mater. Manuf. Innov.* 4 (1) (2015) 10.
- [14] N. Hu, R. Burgueño, Buckling-induced smart applications: recent advances and trends, *Smart Mater. Struct.* 24 (6) (2015) 063001.
- [15] C.G. Diaconu, P.M. Weaver, F. Mattioni, Concepts for morphing airfoil sections using bi-stable laminated composite structures, *Thin-Walled Struct.* 46 (6) (2008) 689–701.
- [16] Y.S. Oh, S. Kota, Synthesis of multistable equilibrium compliant mechanisms using combinations of bistable mechanisms, *J. Mech. Des.* 131 (2) (2009) 021002.
- [17] B. Haghpanah, L. Salari-Sharif, P. Pourjab, J. Hopkins, L. Valdevit, Multistable shape-reconfigurable architected materials, *Adv. Mater.* 28 (36) (2016) 7915–7920.
- [18] C. Findeisen, J. Hohe, M. Kadic, P. Gumbsch, Characteristics of mechanical metamaterials based on buckling elements, *J. Mech. Phys. Solids* 102 (2017) 151–164.
- [19] K. Che, C. Yuan, H.J. Qi, J. Meaud, Viscoelastic multistable architected materials with temperature-dependent snapping sequence, *Soft Matter* 14 (13) (2018) 2492–2499.
- [20] G. Simitses, D.H. Hodges, *Fundamentals of Structural Stability*, Butterworth-Heinemann, 2006.
- [21] Q. Chen, X. Zhang, B. Zhu, Design of buckling-induced mechanical metamaterials for energy absorption using topology optimization, *Struct. Multidiscip. Optim.* 58 (4) (2018) 1395–1410.
- [22] P. Cazottes, A. Fernandes, J. Pouget, M. Hafez, Bistable buckled beam: modeling of actuating force and experimental validations, *J. Mech. Des.* 131 (10) (2009) 101001.
- [23] T. Chen, J. Mueller, K. Shea, Integrated design and simulation of tunable, multi-state structures fabricated monolithically with multi-material 3D printing, *Sci. Rep.* 7 (2017) 45671.
- [24] D. Restrepo, N.D. Mankame, P.D. Zavattieri, Phase transforming cellular materials, *Extreme Mech. Lett.* 4 (2015) 52–60.
- [25] S. Shan, S.H. Kang, J.R. Raney, P. Wang, L. Fang, F. Candido, J.A. Lewis, K. Bertoldi, Multistable architected materials for trapping elastic strain energy, *Adv. Mater.* 27 (29) (2015) 4296–4301.
- [26] K. Che, C. Yuan, J. Wu, H.J. Qi, J. Meaud, Three-dimensional-printed multistable mechanical metamaterials with a deterministic deformation sequence, *J. Appl. Mech.* 84 (1) (2017) 011004.
- [27] T. Frenzel, C. Findeisen, M. Kadic, P. Gumbsch, M. Wegener, Tailored buckling microlattices as reusable light-weight shock absorbers, *Adv. Mater.* 28 (28) (2016) 5865–5870.
- [28] X. Tan, B. Wang, S. Chen, S. Zhu, Y. Sun, A novel cylindrical negative stiffness structure for shock isolation, *Compos. Struct.* 214 (2019) 397–405.
- [29] H. Yang, L. Ma, Multi-stable mechanical metamaterials with shape-reconfiguration and zero poisson's ratio, *Mater. Des.* 152 (2018) 181–190.
- [30] M. Santer, S. Pellegrino, Concept and design of a multistable plate structure, *J. Mech. Des.* 133 (8) (2011) 081001.
- [31] A. Rafsanjani, A. Akbarzadeh, D. Pasini, Snapping mechanical metamaterials under tension, *Adv. Mater.* 27 (39) (2015) 5931–5935.
- [32] B. Camescasse, A. Fernandes, J. Pouget, Bistable buckled beam: elastica modeling and analysis of static actuation, *Int. J. Solids Struct.* 50 (19) (2013) 2881–2893.
- [33] M. Vangbo, An analytical analysis of a compressed bistable buckled beam, *Sensors Actuators A* 69 (3) (1998) 212–216.